Axion Minicluster Streams in the Solar Neighborhood

Ciaran A. J. O'Hare[1,*] Giovanni Pierobon,[2,†] and Javier Redondo[3,4,‡]
[1]School of Physics, Physics Road, The University of Sydney, New South Wales 2006 Camperdown, Sydney, Australia
[2]School of Physics, The University of New South Wales, New South Wales 2052 Kensington, Sydney, Australia
[3]CAPA & Departamento de Fisica Teorica, Universidad de Zaragoza, 50009 Zaragoza, Spain
[4]Max-Planck-Institut für Physik (Werner-Heisenberg-Institut), Föhringer Ring 6, 80805 München, Germany

(Received 15 January 2024; accepted 19 July 2024; published 21 August 2024)

A consequence of QCD axion dark matter being born after inflation is the emergence of small-scale substructures known as miniclusters. Although miniclusters merge to form minihalos, this intrinsic granularity is expected to remain imprinted on small scales in our galaxy, leading to potentially damaging consequences for the campaign to detect axions directly on Earth. This picture, however, is modified when one takes into account the fact that encounters with stars will tidally strip mass from the miniclusters, creating pc-long tidal streams that act to refill the dark matter distribution. Here we ask whether or not this stripping rescues experimental prospects from the worst-case scenario in which the majority of axions remain bound up in unobservably small miniclusters. We find that the density sampled by terrestrial experiment on mpc scales will be, on average, around 70%–90% of the average local DM density, and at a typical point in the solar neighborhood, we expect most of the dark matter to be comprised of debris from $\mathcal{O}(10^2$–$10^3)$ overlapping streams. If haloscopes can measure the axion signal with high-enough frequency resolution, then these streams are revealed in the form of an intrinsically spiky line shape, in stark contrast with the standard assumption of a smooth, featureless Maxwellian distribution—a unique prediction that constitutes a way for experiments to distinguish between pre- and postinflationary axion cosmologies.

DOI: 10.1103/PhysRevLett.133.081001

Introduction—Axions [1–9] are one of the most popular explanations for the makeup of galactic dark matter (DM) halos (for reviews, see, e.g., [10–15]). There are several well-motivated cosmological production scenarios for axion DM, but one of the most interesting and predictive examples is when the symmetry-breaking phase transition that births the axion occurs *after* inflation. Dedicated numerical simulations studying this scenario have flourished in recent years [16–23].

It has been known for many years [24–26] that the complicated multiscale dynamics of the axion field that necessitate the constriction of these simulations, also implies that the DM distribution in this scenario will inherit inhomogeneities on scales set by the horizon at the QCD phase transition. This results in the majority of DM becoming bound inside planetary-mass structures called *miniclusters* [24–37]. To put it plainly: miniclusters would be too sparsely distributed for us to have a realistic chance of encountering one, so prospects for detecting DM axions in the lab rest upon whether or not miniclusters survive in our galaxy today.

In this Letter, we address the detectability of DM axions by quantifying their distribution in the solar neighborhood. Broadly speaking, DM in this scenario can be thought of in terms of three distinct populations. First, there are the axions that never end up inside miniclusters to begin with, existing instead in the "minivoids" between them [38]. Second, there are the miniclusters themselves, which lock up more than 80% of the mass of DM prior to galaxy formation [39]. Lastly, there is the minicluster debris—axions tidally stripped from their hosts as they orbit the Milky Way (MW) [40–44]. The worst-case scenario for direct detection experiments (referred to as "haloscopes") is if we consider the axions only from the minivoids [38]. However, tidal disruption will act to spread the DM across a wider volume [40], so observational prospects could be rescued if we account for this.

To that end, we have performed Monte Carlo simulations that begin with a realistic population of miniclusters taken from early-Universe simulations, and are then evolved as they orbit the MW. For each minicluster, we calculate how much mass is stripped from it, and over what length scale this mass is spread so that we can build a model for the resulting stream network. Figure 1 shows an illustration of

*Contact author: ciaran.ohare@sydney.edu.au
†Contact author: g.pierobon@unsw.edu.au
‡Contact author: jredondo@unizar.es

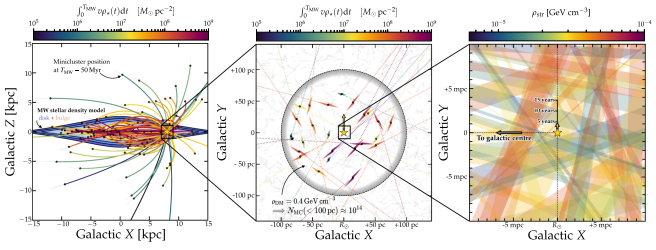

FIG. 1. Schematic of our study. Left: We begin by modeling the orbits of many miniclusters all ending at the Solar position today, $(X, Y, Z) \approx (8, 0, 0)$ kpc. For each orbit, we draw random encounters with stars from a MW stellar density model that includes the thin and thick disks, and the bulge. We color the minicluster orbits by the integral of this density along the orbit. For clarity, we display only the last 50 Myr of the orbit. Center: Enlarging a 100-pc-radius sphere around the Sun, we illustrate how the axions stripped from their host minicluster are elongated into tidal streams of $\mathcal{O}(\mathrm{pc})$ length. Right: Enlargement $\sim$ mpc scales relevant for experiments where the network of tidal streams sums to give the local density in axions.

the stages of this calculation. We then use these results to create example haloscope signals, as in Fig. 2.

Initial miniclusters—To start our calculation, we need to know the initial distribution of minicluster masses and density profiles. We source this information from the most recent N-body simulations of minicluster formation, which themselves begin from initial conditions left over from lattice simulations of axions around the QCD phase transition [45]. The most pertinent result of these

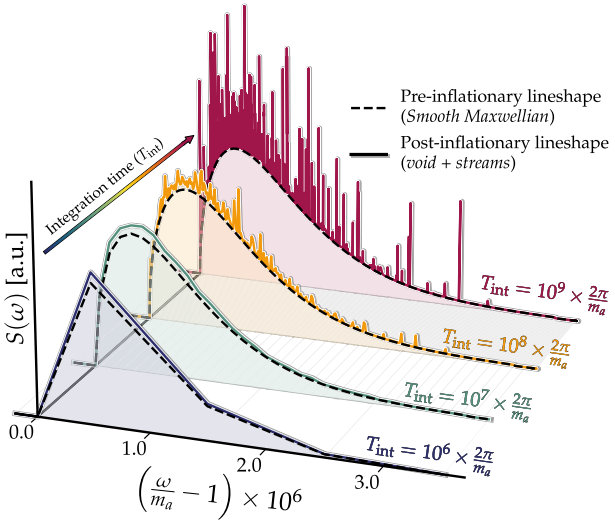

FIG. 2. An illustration of how minicluster streams would manifest in the experimental signature of axions called the"line shape." The frequency resolution is inversely proportional to the duration of the observation, $T_{\rm int}$, from which this spectrum is obtained via a discrete Fourier transform. If $T_{\rm int}$ is short, then the line shape is indistinguishable from a smooth halo. However, samples longer than $\sim 10^8$ oscillation periods have sufficient resolution to identify the streams.

simulations is the two types of miniclusters that form—what we refer to as *merged* miniclusters, and *isolated* miniclusters. The former result from hierarchical merging and develop Navarro-Frenk-White (NFW) density profiles [45–47], while the latter form from the prompt collapse of isolated overdensities and then do not undergo many substantial mergers—retaining the power-law profiles usually associated with self-similar collapse, $\rho \propto r^{-\tilde{\alpha}}$ [27]. In our baseline set of results, we adopt $\tilde{\alpha} = 2.71$ taken from fitting their density profiles at the latest times in our simulation [45].

Isolated miniclusters are the most abundant, however, they collectively make up very little of the total DM since they have masses $M \lesssim 10^{-12} M_\odot$. Merged miniclusters, on the other hand, have masses $M \gtrsim 10^{-12} M_\odot$, so comprise most of the DM by mass. We draw minicluster masses from a broken power-law mass function representing these two populations: $\mathrm{d}n/\mathrm{d}\log M \propto M^\gamma$, with $\gamma = -0.8$ for isolated miniclusters between $[10^{-16}, 10^{-12}] M_\odot$, and $\gamma = -0.5$ for merged minihalos up to $5 \times 10^{-7} M_\odot$. We discuss N-body results and justify these inputs in the Supplemental Material [48], Sec. I, which includes Refs. [49–66].

Monte Carlo simulation—After drawing a sample of miniclusters, we propagate their orbits around the galaxy. We are interested here in the set of all possible galactic orbits that end in the Solar neighborhood today. Velocities are sampled according to the standard halo model (SHM) by drawing from an isotropic 3D Gaussian with width $\sigma_{\rm halo} = v_{\rm circ}/\sqrt{2}$, where $v_{\rm circ} = 233$ km/s is the circular speed of the Solar orbit [67]. We truncate the velocity distribution at $v_{\rm esc} = 528$ km/s [68] to discount orbits unbound to the MW. We integrate orbits over a duration $t_{\rm MW} = 13.5$ Gyr using GALPY [69], adopting the commonly used potential "MWPotential2014."

For each orbit, we evaluate the variation in the local stellar number density $n_\star(t)$ felt by the minicluster. Our Galactic model includes a central bulge and the thin or thick disks—described in Supplemental Material [48], Sec. II. The total number of stars encountered by the minicluster is the integral,

$$N_{\rm enc} = \int_0^{t_{\rm MW}} \mathrm{d}t n_\star(t) v(t) \pi b_{\rm max}^2, \tag{1}$$

where $v(t)$ is the minicluster velocity, and $b_{\rm max}$ some maximum impact parameter between the minicluster and a star. We want to set $b_{\rm max}$ to be as large as possible to capture all possible disruption but without being so large as to add unnecessary computational burden by having large numbers of negligible encounters. As in Ref. [42], we find that $b_{\rm max} = 0.1$ pc strikes a good balance. Increasing this number by a factor of 10 does not change our results. The $N_{\rm enc}$ encounters are labeled by a set of encounter times $\{t_{\rm enc}^i\}$, drawn from a probability distribution proportional to the integrand in Eq. (1). The impact parameter, b of each

encounter, are drawn randomly from inside a circle of radius $b_{\rm max}$.

Stars appear to miniclusters as pointlike objects, which means we may work in the *distant tide* approximation, where the impact parameter between the minicluster and a star is much larger than the minicluster radius, $b \gg R$. The energy injected by an encounter with a star of mass $M_\star$ under this approximation is [70,71],

$$\Delta E \simeq \left(\frac{2GM_\star}{b^2 v_{\rm rel}}\right)^2 \frac{M\langle R^2\rangle}{3}, \tag{2}$$

where $v_{\rm rel}$ is the minicluster-star relative velocity, and $\langle R^2\rangle$ is the minicluster mean-squared radius (see Supplemental Material [48], Sec. III for how the latter is calculated). Most encounters inject $\Delta E \ll E_b$ so we must deal with *perturbations*, which do not totally disrupt the minicluster in one go, but lead to a series of mass losses ΔM^i. The procedure then is to execute $i = 1, \ldots, N_{\rm enc}$ successive perturbations over the minicluster's orbit, repeatedly updating the mass and radius that it relaxes to, until it is either fully unbound or we reach the end of the orbit. The recipe for this procedure is given in Supplemental Material [48], Sec. III. For computational efficiency, we group together the very large number of encounters occurring during a disk-crossing event, and only allow the minicluster to relax to a new profile and radius over its relaxation time between disk crossings. This is justified here because the relaxation time $[t_{\rm rel} \sim (G\rho_{\rm mc})^{-1/2} \sim \mathcal{O}(10\ {\rm Myr})]$ is shorter than the timescale between disk crossings where major encounters occur: $\mathcal{O}$(10–100 Myr).

We find that isolated miniclusters are relatively stable against disruption, and the majority survive with some mass intact. The high-mass merged miniclusters are much more easily disrupted, with around half of them losing $> 99\%$ of their mass by today.

Stream formation—When a certain amount of the minicluster's mass is stripped, where does it go? Although this unbound mass shell has effectively evaporated off of the minicluster, it will still retain its host's center-of-mass orbital velocity, and so continue along the same orbit in the vicinity. The tidal field of the Milky Way will continue to act on these unbound particles, causing the debris to elongate into a stream in the direction of the orbit. This is seen generically for tidally disrupted structures at all scales in astrophysics, but has also been simulated for DM microhalos on the scales we are interested in here in Ref. [71]. We use this study as inspiration for our stream model. We assume that an unbound mass shell turns into a tidal stream, with a leading tail that advances beyond the original host minicluster and a trailing tail that lags behind. By today, a given mass shell evaporating in some encounter at time $t^i_{\rm enc}$ will have turned into a stream of *minimum* length given by the minicluster velocity dispersion [71], $\ell^i_{\rm str} \gtrsim \sigma^i_{\rm mc}(t_{\rm MW} - t^i_{\rm enc})$. It is important to note that the stream will likely be longer than this today due to the energy injection and further tidal heating, potentially by a factor of 10 compared to $\sim\sigma_{\rm mc} t$ [71]. We explore levels of additional elongation in Supplemental Material [48], Sec. IV, but for reasons that will become clear, taking the smallest possible length that the streams could grow to is the most conservative option for the question we are trying to answer.

To model the stream formation, we will make the assumption that the mass lost in each tidal disruption event goes into a cylinder the same radius as the original minicluster, R, and with a Gaussian density profile running along the stream. The total stream is then comprised of the sum of all of these individual evaporated mass shells occurring at different times. We can parametrize this in terms of a function $\rho_{\rm str}(\ell)$,

$$\rho_{\rm str}(\ell) = \sum_{i=1}^{N_{\rm enc}} \frac{\Delta M^i}{\pi R^2_{\rm mc}\sqrt{2\pi(\ell^i_{\rm str})^2}} \exp\left(-\frac{\ell^2}{2(\ell^i_{\rm str})^2}\right), \tag{3}$$

where ℓ is a coordinate that runs along the stream. The length scales for the miniclusters (weighted by the ΔM in each segment) are in the range $7.3^{+3.2}_{-4.0}$ pc for merged miniclusters and $0.28^{+0.34}_{-0.2}$ pc for isolated miniclusters.

The local density in minicluster streams—We will now present an argument for the degree to which the local DM density at our position in the galaxy is replenished by the disruption of the miniclusters into long streams. First, imagine a sphere around the Sun of radius 100 pc. This is the order-of-magnitude scale within which we have strong evidence for a galactic DM density of $\rho_{\rm DM} \approx 0.4\ {\rm GeV/cm^3} \approx 0.01 M_\odot\ {\rm pc}^{-3}$ [72]. Within this sphere, the total mass of DM is $M_{\rm DM} = 4.2 \times 10^4 M_\odot$. From Ref. [38], we know around $f_{\rm void} = 8\%$ of this should be comprised of an ambient density of unbound axions—the minivoids. Therefore $M_{\rm DM}(1 - f_{\rm void})$ is the total mass of axions that were initially bound in miniclusters inside this volume. Using our baseline mass function, this implies a total of around $N_{\rm mc} \sim 10^{14}$ isolated + merged miniclusters.

Let us assume the final volume occupied by each stream after the disruption process is $V_{\rm str} \approx \pi R^2_{\rm mc} l_{95}$. We define l_{95} to be the length within which 95% of the stream mass is contained, calculated using Eq. (3). If we have $N_{\rm mc}$ miniclusters inside a volume $V = 4/3\pi r^3_{\rm local}$ and those miniclusters each occupy a volume $V_{\rm str}$ after disruption, the expected number of streams overlapping a random point inside the sphere is then

$$\langle N_{\rm str}\rangle = \sum_{j=1}^{N_{\rm mc}} \frac{V^j_{\rm str}}{V_{\rm local}}, \tag{4}$$

where the ratio of the two volumes gives us the probability that a particular stream overlaps our chosen point. For our baseline set of assumptions, we find that this number is

246 ± 15 (statistical error). Varying our assumptions—for example the density profiles, the concentration of the NFW merged miniclusters, and/or accounting for additional stream heating—we obtain numbers in the range ~200 to 6000, see Supplemental Material [48], Sec. IV.

With this number, we can now resample from our distribution of streams $\mathcal{O}(10^2$–$10^3)$ times, with probabilities weighted by $V^i_{\rm str}$. For each stream, we also randomly choose our position within it $\ell \in [-l_{95}/2, l_{95}/2]$ to get the value of the DM density that it contributes from Eq. (3). Repeating this process many times, we find that the sum of all the individual densities adds up to a total

$$\frac{1}{\rho_{\rm DM}} \sum_{i=1}^{N_{\rm str}} \rho^i_{\rm str}(\ell^i_\odot) = 0.81 \pm 0.06, \tag{5}$$

where $\rho_{\rm DM} \approx 0.4\ {\rm GeV/cm^3}$ is the usual DM density inferred on much larger scales. So when added to the 8% of the DM density originally filling the minivoids, this is a replenishment of almost 90% of $\rho_{\rm DM}$—a substantial improvement in the prospects for direct detection.

We emphasize here that this final number is generally insensitive to many of our cruder assumptions. The first point to state is that the debris from disrupted miniclusters is dominated almost entirely by the *merged* ones. These streams constitute the most DM by mass, and have the highest probability of intersecting our position because they cover more volume.

The second key point is that the expected value of the DM density [Eq. (5)] is robust against reparametrizations as long as we are in the regime when $N_{\rm str} \gg 1$. That said, the number of expected streams is somewhat arbitrary, but given that it is very safely $\gg 1$ for any reasonable choice of parameters, we show explicitly in Supplemental Material [48], Sec. IV that the typical (i.e., median, or mean) DM density they add up to does not depend on this number because we have conserved the total DM mass. Instead, the number of streams affects the *variance* in $\rho_{\rm str}$. It can also be shown (see Supplemental Material [48], Sec. IV) that as long as the minicluster mass and radius are related like $R \propto M^{1/3}$ then the mass dependence drops out entirely, meaning assumptions about the mass function also do not affect $N_{\rm str}$, leaving only a dependence on the NFW concentration parameter.

Quantities that affect $N_{\rm str}$ include the typical radii that the miniclusters are truncated at (related to the concentration parameter for NFW profiles), and the extent to which streams are additionally elongated beyond the minimal expectation $\sigma_{\rm mc} t$. If we allow the miniclusters to be larger in radius, or the streams to be longer, then the typical number of streams overlapping at our position increases to $\mathcal{O}(10^3)$—however, this means that the variance in the mean density our position ends up *smaller*. Because of this, our baseline parametrization is the most conservative—allowing for processes that can further strip the miniclusters or elongate streams only acts to suppress the variation in the value stated in Eq. (5). Figure S3 in the Supplemental Material [48] shows the impact of these uncertainties quantitatively.

Put together, the only uncertainty remaining that could change our results substantially is if the merged miniclusters do not continue to evolve towards smooth NFW profiles: If instead some of them remain as "clusters of miniclusters," then it is possible that they are more resilient. We discuss this issue in Supplemental Material [48], Sec. V. The takeaway from our N-body simulation halo finder is that the majority of the axions inside merged miniclusters are indeed attached to their host halo as opposed to internal subhalos.

Impact on axion haloscopes—We now know how many streams we expect to have around us at any one time, and so we can draw a sample of this size and predict how this would look in a haloscope. First, we build the velocity distribution of axions. In the voids, we can safely assume the halo is described by the smooth, fully virialized SHM [67] modeled as an isotropic Gaussian with width $\sigma_{\rm void} = v_{\rm circ}/\sqrt{2} \approx 165$ km/s. An experiment observes this after a Galilean boost into our frame of reference, moving at a velocity $\mathbf{v}_{\rm lab}(t)$ with respect to the Galactic center. We take $\mathbf{v}_{\rm lab} = (11.1, 235.2, 7.3)\ {\rm km/s} + \mathbf{v}_\oplus(t)$ [67] in the same galactocentric coordinate system as Fig. 1, where $\mathbf{v}_\oplus(t)$ is the Earth velocity, see, e.g., [73,74].

Following past literature [75–80], we take the stream velocity distribution to have the same Gaussian form, except we boost by $\mathbf{v}_{\rm lab} - \mathbf{v}_{\rm str}$ to account for the stream's velocity, and set the width to $\sigma_{\rm str}$. Because the values of $\sigma_{\rm str}$ are small, the stream signals are extremely narrow band in frequency.

We now relate this velocity distribution to the signal measured by a typical axion haloscope known as the *line shape*. The axion field's oscillations are highly coherent, in keeping with its description as cold DM. Within a "coherence time," the axion field will appear to oscillate at a single frequency $\omega \approx m_a(1 + v^2/2)$, where $v \sim 10^{-3}c$ is some speed drawn from $f(v)$. This frequency will then evolve on timescales longer than coherence time, depending on the spread in velocities: $\tau_{\rm coh} \sim 1/m_a\sigma^2_{\rm void} \sim 10^6 m_a^{-1} \sim 0.01\ {\rm ms}(100\ \mu{\rm eV}/m_a)$. If oscillations are measured over timescales much longer than this, then the discrete Fourier transform of that measurement will have a spectrum related to the distribution of component frequencies. For a measurement time, $T_{\rm int}$, the power spectrum $S(\omega)$ has a frequency resolution of $\Delta\omega = 2\pi/T_{\rm int}$. Therefore, if $T_{\rm int} > 10^6 \times 2\pi/m_a$ (i.e., longer than a million oscillation periods) then we expect the axion's line shape to be resolved [77,81–83].

To illustrate this, we construct a simplified version of a signal power spectrum by discretizing the distribution of frequencies into bins of width $\Delta\omega$ [77,83,84]. Figure 2 compares the smooth Maxwellian case (as in, for example,

preinflationary axions) against the case where there are streams in the signal. The two will become strikingly different once the signal is integrated for timescales longer than 10^8 oscillation periods.

As well as showing up as sharp features in short-duration measurements, the line shape will also evolve in amplitude over human timescales as we traverse the streams. Sampling over all of our streams and randomizing our trajectory through them, we find that they would typically persist for around $\Delta t = 30^{+23}_{-11}$ yr (median and 68% containment). However, since we expect 10^2–10^3 present in the line shape at one time, the timescale over which the signal is expected to vary is on the order of weeks. Ultra-narrowband axion signals like these are already being searched for by haloscope collaborations [85–87], so in light of our results, we advocate that these efforts continue.

Conclusions—We have evaluated the extent to which axion haloscopes are doomed to never discover the axion in the postinflationary scenario because axions find themselves bound up inside of small substructures. By modeling the tidal disruption of these miniclusters by stars, we have found that the density of DM around us in the solar neighborhood is refilled to around 80% of the 100-pc-scale average density value $\rho_{\rm DM} \approx 0.4\ {\rm GeV\,cm^{-3}}$ usually adopted by experiments. Combined with an estimate of the leftover density of DM in minivoids [38], this boosts the signal up to an impressive 90% of the commonly assumed value. In other words: axion haloscopes may not be doomed.

Acknowledgments—We give special thanks to Chris Gordon and Ian DSouza for pointing out critical typos in the original version of this Letter. We also thank Benedikt Eggemeier, David Marsh, and Yvonne Wong for helpful discussions. C. A. J. O. is funded via the Australian Research Council, Grant No. DE220100225. The work of J. R. is supported by Grants No. PGC2022-126078NB-C21 funded by MCIN/AEI/ and "ERDF A way of making Europe," and Grant DGA-FSE Grant No. 2020-E21-17R Aragon Government and the European Union—NextGenerationEU Recovery and Resilience Program on "Astrofísica y Física de Altas Energías" CEFCA-CAPA-ITAINNOVA. This Letter is based upon work from COST Action COSMIC WISPers CA21106, supported by COST (European Cooperation in Science and Technology).

[1] R. D. Peccei and H. R. Quinn, *CP* conservation in the presence of instantons, Phys. Rev. Lett. **38**, 1440 (1977).
[2] R. D. Peccei and H. R. Quinn, Constraints imposed by *CP* conservation in the presence of instantons, Phys. Rev. D **16**, 1791 (1977).
[3] S. Weinberg, A new light boson?, Phys. Rev. Lett. **40**, 223 (1978).
[4] F. Wilczek, Problem of strong *P* and *T* invariance in the presence of instantons, Phys. Rev. Lett. **40**, 279 (1978).
[5] J. E. Kim and G. Carosi, Axions and the strong *CP* problem, Rev. Mod. Phys. **82**, 557 (2010); **91**, 049902(E) (2019).
[6] J. E. Kim, Weak interaction singlet and strong *CP* invariance, Phys. Rev. Lett. **43**, 103 (1979).
[7] M. A. Shifman, A. I. Vainshtein, and V. I. Zakharov, Can confinement ensure natural *CP* invariance of strong interactions?, Nucl. Phys. **B166**, 493 (1980).
[8] M. Dine, W. Fischler, and M. Srednicki, A simple solution to the strong *CP* problem with a harmless axion, Phys. Lett. **104B**, 199 (1981).
[9] A. R. Zhitnitsky, On possible suppression of the axion hadron interactions. (In Russian), Yad. Fiz. **31**, 497 (1980) [Sov. J. Nucl. Phys. **31**, 260 (1980)].
[10] L. Di Luzio, M. Giannotti, E. Nardi, and L. Visinelli, The landscape of QCD axion models, Phys. Rep. **870**, 1 (2020).
[11] F. Chadha-Day, J. Ellis, and D. J. E. Marsh, Axion dark matter: What is it and why now?, Sci. Adv. **8**, abj3618 (2022).
[12] I. G. Irastorza and J. Redondo, New experimental approaches in the search for axion-like particles, Prog. Part. Nucl. Phys. **102**, 89 (2018).
[13] Y. K. Semertzidis and S. Youn, Axion dark matter: How to see it?, Sci. Adv. **8**, abm9928 (2022).
[14] C. B. Adams *et al.*, Axion dark matter, in *2022 Snowmass Summer Study* (2022), arXiv:2203.14923.
[15] C. A. J. O'Hare, Cosmology of axion dark matter, Proc. Sci. COSMICWISPers (2024) 040.
[16] L. Fleury and G. D. Moore, Axion dark matter: Strings and their cores, J. Cosmol. Astropart. Phys. 01 (2016) 004.
[17] V. B. Klaer and G. D. Moore, The dark-matter axion mass, J. Cosmol. Astropart. Phys. 11 (2017) 049.
[18] A. Vaquero, J. Redondo, and J. Stadler, Early seeds of axion miniclusters, J. Cosmol. Astropart. Phys. 04 (2019) 012.
[19] M. Gorghetto, E. Hardy, and G. Villadoro, Axions from strings: The attractive solution, J. High Energy Phys. 07 (2018) 151.
[20] M. Buschmann, J. W. Foster, and B. R. Safdi, Early-universe simulations of the cosmological axion, Phys. Rev. Lett. **124**, 161103 (2020).
[21] M. Gorghetto, E. Hardy, and G. Villadoro, More axions from strings, SciPost Phys. **10**, 050 (2021).
[22] M. Buschmann, J. W. Foster, A. Hook, A. Peterson, D. E. Willcox, W. Zhang, and B. R. Safdi, Dark matter from axion strings with adaptive mesh refinement, Nat. Commun. **13**, 1049 (2022).
[23] C. A. J. O'Hare, G. Pierobon, J. Redondo, and Y. Y. Y. Wong, Simulations of axionlike particles in the postinflationary scenario, Phys. Rev. D **105**, 055025 (2022).
[24] C. J. Hogan and M. J. Rees, Axion miniclusters, Phys. Lett. B **205**, 228 (1988).
[25] E. W. Kolb and I. I. Tkachev, Large amplitude isothermal fluctuations and high density dark matter clumps, Phys. Rev. D **50**, 769 (1994).
[26] E. W. Kolb and I. I. Tkachev, Femtolensing and picolensing by axion miniclusters, Astrophys. J. Lett. **460**, L25 (1996).
[27] K. M. Zurek, C. J. Hogan, and T. R. Quinn, Astrophysical effects of scalar dark matter miniclusters, Phys. Rev. D **75**, 043511 (2007).

[28] E. Hardy, Miniclusters in the axiverse, J. High Energy Phys. 02 (2017) 046.
[29] S. Davidson and T. Schwetz, Rotating drops of axion dark matter, Phys. Rev. D **93**, 123509 (2016).
[30] J. Enander, A. Pargner, and T. Schwetz, Axion minicluster power spectrum and mass function, J. Cosmol. Astropart. Phys. 12 (2017) 038.
[31] N. Blinov, M. J. Dolan, and P. Draper, Imprints of the early universe on axion dark matter substructure, Phys. Rev. D **101**, 035002 (2020).
[32] V. Dandoy, J. Jaeckel, and V. Montoya, Using axion miniclusters to disentangle the axion-photon coupling and the dark matter density, J. Cosmol. Astropart. Phys. 05 (2024) 035.
[33] M. Fairbairn, D. J. E. Marsh, and J. Quevillon, Searching for the QCD axion with gravitational microlensing, Phys. Rev. Lett. **119**, 021101 (2017).
[34] M. Fairbairn, D. J. E. Marsh, J. Quevillon, and S. Rozier, Structure formation and microlensing with axion miniclusters, Phys. Rev. D **97**, 083502 (2018).
[35] D. Croon, D. McKeen, and N. Raj, Gravitational microlensing by dark matter in extended structures, Phys. Rev. D **101**, 083013 (2020).
[36] D. Ellis, D. J. E. Marsh, B. Eggemeier, J. Niemeyer, J. Redondo, and K. Dolag, Structure of axion miniclusters, Phys. Rev. D **106**, 103514 (2022).
[37] T. D. P. Edwards, B. J. Kavanagh, L. Visinelli, and C. Weniger, Transient radio signatures from neutron star encounters with QCD axion miniclusters, Phys. Rev. Lett. **127**, 131103 (2021).
[38] B. Eggemeier, C. A. J. O'Hare, G. Pierobon, J. Redondo, and Y. Y. Y. Wong, Axion minivoids and implications for direct detection, Phys. Rev. D **107**, 083510 (2023).
[39] B. Eggemeier, J. Redondo, K. Dolag, J. C. Niemeyer, and A. Vaquero, First simulations of axion minicluster halos, Phys. Rev. Lett. **125**, 041301 (2020).
[40] P. Tinyakov, I. Tkachev, and K. Zioutas, Tidal streams from axion miniclusters and direct axion searches, J. Cosmol. Astropart. Phys. 01 (2016) 035.
[41] V. I. Dokuchaev, Y. N. Eroshenko, and I. I. Tkachev, Destruction of axion miniclusters in the galaxy, Sov. J. Exp. Theor. Phys. **125**, 434 (2017).
[42] B. J. Kavanagh, T. D. P. Edwards, L. Visinelli, and C. Weniger, Stellar disruption of axion miniclusters in the Milky Way, Phys. Rev. D **104**, 063038 (2021).
[43] I. DSouza and C. Gordon, The disruption of dark matter minihalos by successive stellar encounters, Phys. Rev. D **109**, 123035 (2024).
[44] X. Shen, H. Xiao, P. F. Hopkins, and K. M. Zurek, Disruption of dark matter minihaloes in the Milky Way environment: Implications for axion miniclusters and early matter domination, Astrophys. J. **962**, 9 (2024).
[45] G. Pierobon, J. Redondo, K. Saikawa, A. Vaquero, and G. D. Moore, Miniclusters from axion string simulations, arXiv:2307.09941.
[46] B. Eggemeier and J. C. Niemeyer, Formation and mass growth of axion stars in axion miniclusters, Phys. Rev. D **100**, 063528 (2019).
[47] H. Xiao, I. Williams, and M. McQuinn, Simulations of axion minihalos, Phys. Rev. D **104**, 023515 (2021).
[48] See Supplemental Material at http://link.aps.org/supplemental/10.1103/PhysRevLett.133.081001 for further detail on our analysis procedure, including the galactic stellar density model, the axion minicluster mass function, and the Monte-Carlo disruption simulation. It also provides further results that support the assumptions made in the manuscript, such as the minicluster stream velocity dispersion and level of minicluster substructure.
[49] J. Spitzer, Lyman, Disruption of Galactic clusters, Astrophys. J. **127**, 17 (1958).
[50] V. Springel, R. Pakmor, O. Zier, and M. Reinecke, Simulating cosmic structure formation with the GADGET-4 code, Mon. Not. R. Astron. Soc. **506**, 2871 (2021).
[51] F. Jiang and F. C. van den Bosch, Statistics of dark matter substructure—I. Model and universal fitting functions, Mon. Not. R. Astron. Soc. **458**, 2848 (2016).
[52] F. C. van den Bosch, G. Tormen, and C. Giocoli, The mass function and average mass loss rate of dark matter subhaloes, Mon. Not. R. Astron. Soc. **359**, 1029 (2005).
[53] W. Dehnen and J. Binney, Mass models of the Milky Way, Mon. Not. R. Astron. Soc. **294**, 429 (1998).
[54] N. Bissantz and O. Gerhard, Spiral arms, bar shape and bulge microlensing in the Milky Way, Mon. Not. R. Astron. Soc. **330**, 591 (2002).
[55] J. Binney, O. Gerhard, and D. Spergel, The photometric structure of the inner galaxy, Mon. Not. R. Astron. Soc. **288**, 365 (1997).
[56] J. L. Zagorac, E. Kendall, N. Padmanabhan, and R. Easther, Soliton formation and the core-halo mass relation: An eigenstate perspective, Phys. Rev. D **107**, 083513 (2023).
[57] M. Nori and M. Baldi, Scaling relations of fuzzy dark matter haloes—I. Individual systems in their cosmological environment, Mon. Not. R. Astron. Soc. **501**, 1539 (2021).
[58] H. Y. J. Chan, E. G. M. Ferreira, S. May, K. Hayashi, and M. Chiba, The diversity of core-halo structure in the fuzzy dark matter model, Mon. Not. R. Astron. Soc. **511**, 943 (2022).
[59] H.-Y. Schive, M.-H. Liao, T.-P. Woo, S.-K. Wong, T. Chiueh, T. Broadhurst, and W. Y. P. Hwang, Understanding the core-halo relation of quantum wave dark matter from 3D simulations, Phys. Rev. Lett. **113**, 261302 (2014).
[60] X. Du, D. J. E. Marsh, M. Escudero, A. Benson, D. Blas, C. K. Pooni, and M. Fairbairn, Soliton merger rates and enhanced axion dark matter decay, Phys. Rev. D **109**, 043019 (2024).
[61] J. Chen, X. Du, E. W. Lentz, D. J. E. Marsh, and J. C. Niemeyer, New insights into the formation and growth of boson stars in dark matter halos, Phys. Rev. D **104**, 083022 (2021).
[62] D. G. Levkov, A. G. Panin, and I. I. Tkachev, Gravitational Bose-Einstein condensation in the kinetic regime, Phys. Rev. Lett. **121**, 151301 (2018).
[63] L. Visinelli, S. Baum, J. Redondo, K. Freese, and F. Wilczek, Dilute and dense axion stars, Phys. Lett. B **777**, 64 (2018).
[64] J. F. Navarro, C. S. Frenk, and S. D. M. White, The structure of cold dark matter halos, Astrophys. J. **462**, 563 (1996).
[65] L. Dai and J. Miralda-Escudé, Gravitational lensing signatures of axion dark matter minihalos in highly magnified stars, Astron. J. **159**, 49 (2020).

[66] V. Dandoy, T. Schwetz, and E. Todarello, A self-consistent wave description of axion miniclusters and their survival in the galaxy, J. Cosmol. Astropart. Phys. 09 (2022) 081.
[67] N. W. Evans, C. A. J. O'Hare, and C. McCabe, Refinement of the standard halo model for dark matter searches in light of the Gaia Sausage, Phys. Rev. D **99**, 023012 (2019).
[68] T. Piffl *et al.*, Constraining the galaxy's dark halo with RAVE stars, Mon. Not. R. Astron. Soc. **445**, 3133 (2014).
[69] J. Bovy, GALPY: A PYTHON library for Galactic dynamics, Astrophys. J. Suppl. Ser. **216**, 29 (2015).
[70] A. M. Green and S. P. Goodwin, On mini-halo encounters with stars, Mon. Not. R. Astron. Soc. **375**, 1111 (2007).
[71] A. Schneider, L. Krauss, and B. Moore, Impact of dark matter microhalos on signatures for direct and indirect detection, Phys. Rev. D **82**, 063525 (2010).
[72] P. F. de Salas and A. Widmark, Dark matter local density determination: Recent observations and future prospects, Rep. Prog. Phys. **84**, 104901 (2021).
[73] C. McCabe, The Earth's velocity for direct detection experiments, J. Cosmol. Astropart. Phys. 02 (2014) 027.
[74] F. Mayet *et al.*, A review of the discovery reach of directional Dark Matter detection, Phys. Rep. **627**, 1 (2016).
[75] K. Freese, P. Gondolo, and H. J. Newberg, Detectability of weakly interacting massive particles in the Sagittarius dwarf tidal stream, Phys. Rev. D **71**, 043516 (2005).
[76] C. A. J. O'Hare and A. M. Green, Directional detection of dark matter streams, Phys. Rev. D **90**, 123511 (2014).
[77] J. W. Foster, N. L. Rodd, and B. R. Safdi, Revealing the dark matter halo with axion direct detection, Phys. Rev. D **97**, 123006 (2018).
[78] C. A. J. O'Hare, C. McCabe, N. W. Evans, G. Myeong, and V. Belokurov, Dark matter hurricane: Measuring the S1 stream with dark matter detectors, Phys. Rev. D **98**, 103006 (2018).
[79] C. A. J. O'Hare, N. W. Evans, C. McCabe, G. Myeong, and V. Belokurov, Velocity substructure from Gaia and direct searches for dark matter, Phys. Rev. D **101**, 023006 (2020).
[80] B. R. Ko, Search for the Sagittarius tidal stream of axion dark matter around 4.55 μeV, in *Proceedings of the 2023 European Physical Society Conference on High Energy Physics* (2023), arXiv:2310.20116.
[81] M. S. Turner, Periodic signatures for the detection of cosmic axions, Phys. Rev. D **42**, 3572 (1990).
[82] A. Derevianko, Detecting dark-matter waves with a network of precision-measurement tools, Phys. Rev. A **97**, 042506 (2018).
[83] C. A. J. O'Hare and A. M. Green, Axion astronomy with microwave cavity experiments, Phys. Rev. D **95**, 063017 (2017).
[84] S. Knirck, A. J. Millar, C. A. J. O'Hare, J. Redondo, and F. D. Steffen, Directional axion detection, J. Cosmol. Astropart. Phys. 11 (2018) 051.
[85] L. Duffy, P. Sikivie, D. B. Tanner, S. J. Asztalos, C. Hagmann, D. Kinion, L. J. Rosenberg, K. van Bibber, D. Yu, and R. F. Bradley, Results of a search for cold flows of dark matter axions, Phys. Rev. Lett. **95**, 091304 (2005).
[86] L. D. Duffy, P. Sikivie, D. B. Tanner, S. J. Asztalos, C. Hagmann, D. Kinion, L. J. Rosenberg, K. van Bibber, D. B. Yu, and R. F. Bradley (ADMX Collaboration), A high resolution search for dark-matter axions, Phys. Rev. D **74**, 012006 (2006).
[87] C. Bartram *et al.* (ADMX Collaboration), Non-virialized axion search sensitive to doppler effects in the Milky Way halo, Phys. Rev. D **109**, 083014 (2024).